INTERNATIONAL JOURNAL FOR NUMERICAL METHODS IN FLUIDS, VOL. 5, 561–575 (1985)

NUMERICAL SIMULATION OF THREE-DIMENSIONAL FLOW IN A CAVITY

CHRISTOPHER J. FREITAS*, ROBERT L. STREET†, ANGELOS N. FINDIKAKIS‡ AND JEFFREY R. KOSEFF§

Department of Civil Engineering, Stanford University, Stanford, California 94305, U.S.A.

SUMMARY

Previous three-dimensional simulations of the lid-driven cavity flow have reproduced only the most general features of the flow. Improvements to a finite difference code, REBUFFS, have made possible the first completely successful simulation of the three-dimensional lid-driven cavity flow. The principal improvement to the code was the incorporation of a modified QUICK scheme, a higher-order upwind finite difference formulation. Results for a cavity flow at a Reynolds number of 3200 have reproduced experimentally observed Taylor–Görtler-like vortices and other three-dimensional effects heretofore not simulated. Experimental results obtained from a unique experimental cavity facility validate the calculated results.

KEY WORDS Cavity Flow Incompressible Flow Control-Volume Formulation Navier–Stokes Equations QUICK Convection Scheme Taylor–Görtler Vortices

INTRODUCTION

The numerical simulation of recirculating flows is of critical interest to engineers simply because of the prevalence of this flow type in engineering applications. From a numerical viewpoint, recirculating flows such as the lid-driven cavity flow can serve as ideal prototype non-linear problems for testing the proper operation of fluid dynamic codes, in both two and three dimensions. The lid-driven cavity's geometric simplicity and well-defined flow structures in two dimensions and at low Reynolds numbers have allowed for comparative analysis of several numerical techniques. In general, good agreement exists among these low Reynolds number (i.e. $Re < 400$), two-dimensional solutions.

The three-dimensional lid-driven cavity flow presents new and possibly unforeseen problems to the numericist. These problems result from significant fluid motions in the third axial direction and a very complex flow field at even low Reynolds numbers.[1,2] The previous three-dimensional simulations have reproduced only the most general features of the flow. This fact was highlighted by Koseff *et al.*[3] by whom experiment and simulation were compared. They obtained a complete description of the three-dimensional circulation structure in the lid-driven cavity by flow visualization techniques. These experimental results where then compared to computed results generated by two different numerical codes, one employing finite differences and the other finite elements. Resolution of only the dominant primary circulation cell and corner vortices was obtained, and both codes failed to resolve the experimentally observed Taylor–Görtler-like (TGL) longitudinal vortices.

*Research Assistant
†Professor of Fluid Mechanics and Applied Mathematics
‡Consulting Assistant Professor
§Assistant Professor

0271-2091/85/060561-15$01.50
© 1985 by John Wiley & Sons, Ltd.
Received 21 August 1984
Revised 19 December 1984

The failure of these two codes to resolve the pertinent laminar flow features can be traced to two points, (1) the accuracy of the numerical scheme, and (2) the grid point distribution or spacing. Working from this premise, we made improvements to the finite difference code used in Reference 3 and used a finer grid. This current paper represents, therefore, a continuation of the work begun in Reference 3. The convective term differencing in REBUFFS has been improved from the first-order accurate HYBRID formulation to the third-order accurate QUICK formulation of Leonard.[4,5] This improvement, coupled with a moderate resolution, non-uniform grid, allowed generation of the first successful numerical simulation of a three-dimensional laminar lid-driven cavity flow.

The subsequent sections of this paper discuss, first, the experimental facility and flow visualization techniques. Secondly, a review of the components and features of and improvements to the code REBUFFS is reported. Thirdly, we present the experimental and simulated results for the case of an uniform density, three-dimensional lid-driven cavity flow at a Reynolds number (*Re*) of 3200. Finally, we conclude with a summary of the results and comments on future work.

THE EXPERIMENTAL FACILITY

The experimental facility has been described in detail in References 1 and 2, but for completeness a brief review of the facility is given here. The lid-driven cavity flow facility consists of two rectangular boxes (Figure 1), the upper box containing the belt drive-system that provides the

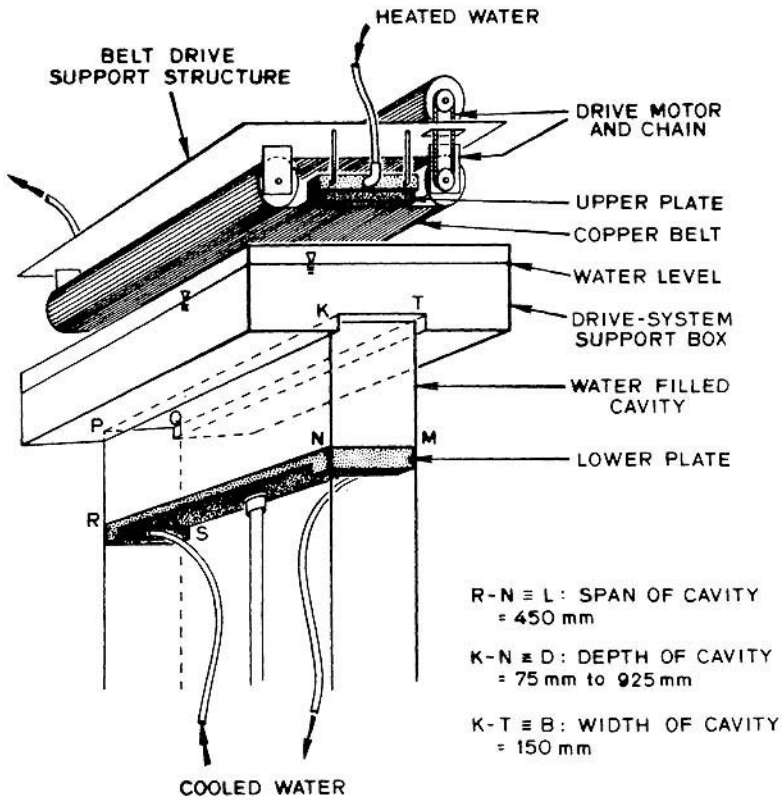

Figure 1. Schematic diagram of lid-driven cavity

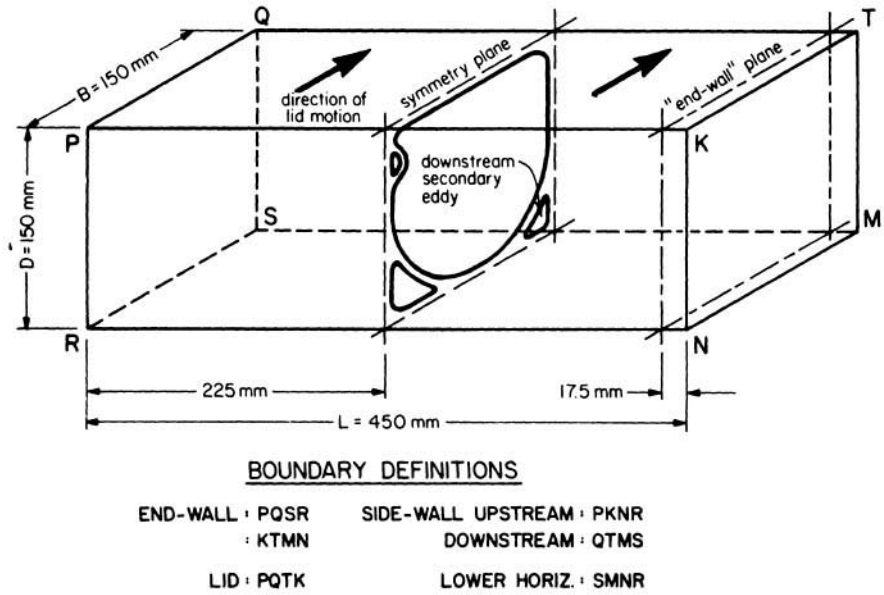

Figure 2. Definitions for lid-driven cavity flow

shear to the top of the lower box (the experimental cavity, region PQTKSMNR in Figure 1) where the recirculating flow occurs. The belt drive-system is composed of a variable speed motor capable of driving the 0·08 mm thick copper belt at selected speeds between 7 mm/s and 230 mm/s (corresponding to a Re range of 1000 to 35,000). The experimental cavity portion of the facility has a width B of 150 mm, a depth D of 150 mm, and a lateral span L of 450 mm. This geometry results in a depth-to-width aspect ratio D/B of 1:1 and a span-to-width aspect ratio L/B of 3:1 (Figure 2). For this cavity the Reynolds number is defined as $Re = VB/\nu$, where V is the belt speed and ν is the average kinematic viscosity of the working fluid, water.

The facility is constructed of 12·5 mm thick Plexiglas; this facilitates flow visualization. The motions of the fluid in this study were visualized by employing the rheoscopic liquid technique as described by Katsaros *et al.*[6] The specific application of this technique to the lid-driven cavity flow facility is described by Rhee *et al.*[2] Briefly, small concentrations of rheoscopic liquid, which consists of extremely small (6 μm × 30 μm × 0·07 μm) plate-like crystalline structures in a water substrate, are evenly distributed in the flow field. The tiny plates align themselves with the shear in the flow and when illuminated by a sheet of laser light they give an instantaneous picture of the flow in any plane. Time exposures of four to eight seconds with a Pentax 35 mm camera were used to obtain well defined pathlines in the flow field.

THE FINITE DIFFERENCE METHOD

The REBUFFS code

The numerical results for this study were produced by a significantly modified version of LeQuere, Humphrey, and Sherman's code REBUFFS (REcirculating BUoyant and Forced Flows Solver).[7] REBUFFS represents an improvement of the TEACH-2E code developed at Imperial College, London by Gosman and Pun[8] and whose fundamentals were laid out by Patankar and Spalding.[9] The TEACH family of codes solve a weak form of the Navier–Stokes equations in

primitive variables via a weighted-residual method (i.e a control-volume formulation). The difference equations are derived according to the TEACH principles by volume integration of the partial differential equations on an elemental volume surrounding each node of the computational grid. The control-volume method specifically used in REBUFFS requires the iterative solution of a set of finite difference equations within a given time step by a line-by-line procedure using a tridiagonal matrix solver. One iteration in REBUFFS consists of the sequential solution of the momentum equations (u, v, w) and a pressure correction equation (a continuity equation). Details of this iterative scheme, which is known by the acronym SIMPLE are presented by Patankar.[10]

Details of the improvements to the original TEACH code, allowing for the development of REBUFFS, are presented by LeQuere *et al.*[7] and were accomplished at the University of California, Berkeley. These improvements include changes to the time-dependent nature of the equations solved and allowance for a strong linkage between the energy and momentum equations through the density dependence on the fluid temperature.

The version of REBUFFS discussed in Reference 3 used the first-order HYBRID scheme in the three-dimensional simulations reported there. HYBRID differencing employs second-order central differencing at nodes where the absolute value of the grid Peclet number is less than or equal to two, and first-order upwind differencing otherwise. Unfortunately, the HYBRID scheme generates tainted flow fields for moderate to large Re flows due to the spurious numerical diffusion introduced by first-order upwinding.[11] This numerical diffusion is undoubtedly responsible for the inadequate three-dimensional results from REBUFFS as presented in Reference 3.

Han *et al.*[12] recognized the weakness of the HYBRID scheme in REBUFFS and implemented Leonard's[4,5] QUICK scheme in two dimensions. QUICK is a third-order accurate upwind differencing scheme which possesses the stability of first-order upwinding but is free of its second-order numerical diffusion. Han *et al.*,[12] though, had difficulty in applying Leonard's formulation and were forced to reformulate and introduce a false-transient term to secure stable solutions. The apparent need for the false-transient term distressed Pollard and Siu.[13] Subsequently, Pollard and Siu developed reformulated versions of QUICK, namely QUICKE and QUICKER, which ensured stable two-dimensional solutions without the need for extra terms.

A modified three-dimensional QUICK formulation

The version of REBUFFS used in this study has also incorporated a QUICK scheme. This version of QUICK ensures that all of the coefficients of the terms in the finite difference expressions are positive and is similar in form to the development of Pollard and Siu.[13] The violation of the condition of all positive (or negative) finite difference coefficients may generate physically unrealistic solutions or divergence of the iterative solution.[10]

In the control-volume formulation, fluxes across the control-volume faces must be computed.

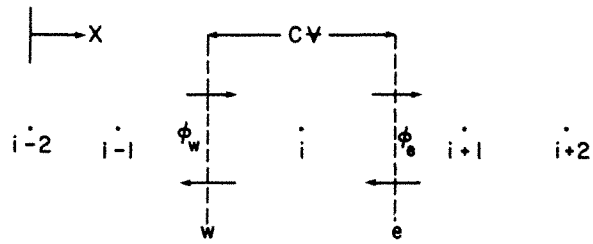

Figure 3(a). Grid point definitions for QUICK

These fluxes represent the integrated convection terms of the partial differential equations. The HYBRID scheme approximates the magnitude of these fluxes by either linearly interpolating the quantity specified at the node points bounding the control-volume face or by setting them equal to the value of the quantity at the node point upstream of the face. The QUICK scheme uses an upstream-weighted quadratic interpolation for these fluxes. As an example of the QUICK formulation used in this study, the one-dimensional flux interpolation equations for a quantity ϕ convected by a velocity field u on a uniform grid (refer to Figure 3(a)) are:

For $u > 0$:

$$\phi_e = \tfrac{1}{8}(6\phi_i - \phi_{i+1} - \phi_{i-1}) + \underset{\text{source}}{\tfrac{1}{2}\phi_{i+1}}, \tag{1}$$

$$\phi_w = \tfrac{1}{8}(6\phi_{i-1} + 3\phi_i) - \underset{\text{source}}{\tfrac{1}{8}\phi_{i-2}}; \tag{2}$$

For $u < 0$:

$$\phi_e = \tfrac{1}{8}(3\phi_i + 6\phi_{i+1}) - \underset{\text{source}}{\tfrac{1}{8}\phi_{i+2}}, \tag{3}$$

$$\phi_w = \tfrac{1}{8}(6\phi_i - \phi_{i+1} - \phi_{i-1}) + \underset{\text{source}}{\tfrac{1}{2}\phi_{i-1}}. \tag{4}$$

These equations are in essence composed of a linear interpolation plus a portion of the respective upstream-weighted second difference normal to the control-volume face.[5] As signified in equations (1)–(4), some terms are incorporated in the source term of the finite difference equations. These additional source terms are necessary to ensure all positive finite difference coefficients and represent one of our most significant modifications to Leonard's[4,5] formulation. In general, the original source term in REBUFFS is comprised of all terms of the partial differential equation except the time dependent term and the convection–diffusion terms. All source terms are evaluated using the current value of the unknown (i.e. lagged one-step in the iterative solution method). This explicit formulation of the source term aids in maintaining the iterative stability of the entire numerical scheme.

The QUICK scheme can be difficult to apply near boundaries and yet previous authors have not commented on their specific applications. REBUFFS uses a staggered grid that requires either one node point outside of or one node point coincident with the boundary of the flow domain.[10] Figure 3(b) displays the situation at an upstream boundary condition where the grid point ϕ_{i-1} coincides with the boundary and ϕ_i represents the first interior node point. When the velocity on the w face of the control-volume is negative (corresponding to equation (4)) then sufficient grid point information exists to evaluate the flux ϕ_w. But, if the velocity is positive (corresponding to equation (2)) then we are unable to compute the magnitude of the flux because the grid point ϕ_{i-2} is not defined. A similar situation develops at a downstream boundary where, in this case, grid point ϕ_{i+2} is not defined. An extrapolation is thus required. After extensive testing a second-order extrapolation was used to represent quantities such as ϕ_{i-2} or ϕ_{i+2} in the flux interpolation equations, namely $\phi_{i-2} = 2\phi_{i-1} - \phi_i$. Higher-order extrapolations produced downwind differences which created unstable solutions. First-order

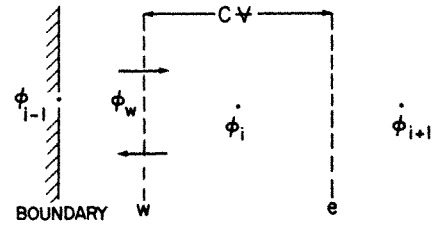

Figure 3(b). Grid point definitions at boundary

extrapolation was numerically stable, but reduced the global accuracy of the algorithm. Thus, a second-order extrapolation is an optimized form for a REBUFFS-type formulation.

In our version of the QUICK scheme the transverse curvature terms, Leonard's CURVT terms, are neglected. Our preliminary tests indicate that elimination of these terms has negligible impact on the computed flow fields; this is confirmed by Leonard.[14] Two consequences of this manipulation are that the convective-terms differencing operator is reduced to second-order accuracy, but the operator has been transformed from a three-dimensional one to a one-dimensional operator. This step eliminates the necessity of an unique formulation in corner boundary regions and simplifies the development of a non-uniform grid version of QUICK.

Finally, our uniform grid version of QUICK was not cost-effective for flows dominated by solid boundaries. In order to resolve the flow near these boundaries and not waste grid points in the interior of the cavity a non-uniform grid version of QUICK was developed and used. The formulation has been simplified to a one-dimensional problem owing to the elimination of the CURVT terms, as discussed above. The development proceeds by determining the coefficients for a general one-dimensional quadratic interpolation equation, for unevenly spaced grid points, i.e. $\phi = c_1 + c_2\xi + c_3\xi^2$, where ξ is the local co-ordinate for a control volume. The general quadratic interpolation equation is then integrated over each control-volume face to generate the corresponding six one-dimensional flux interpolation equations for a non-uniform grid. Equations (1)–(4) become for a non-uniform grid:

For $u > 0$:

$$\begin{aligned}\phi_e = {} & \{\tfrac{1}{2} + \tfrac{1}{4}(x_{i+1} - x_i)/(x_i - x_{i-1})\}\phi_i \\ & - \{\tfrac{1}{4}(x_{i+1} - x_i)/((x_{i+1} - x_i) + (x_i - x_{i-1}))\}\phi_{i+1} \\ & + \{[(\tfrac{1}{2}(x_{i+1} - x_i) + \tfrac{1}{4}(x_{i+1} - x_i)^2/(x_i - x_{i-1}))/ \\ & \quad ((x_{i+1} - x_i) + (x_i - x_{i-1}))] \\ & - \tfrac{1}{2}(x_{i+1} - x_i)/(x_i - x_{i-1})\}\phi_{i-1} + \underset{\text{source}}{\tfrac{1}{2}\phi_{i+1}},\end{aligned} \tag{5}$$

$$\begin{aligned}\phi_w = {} & \{\tfrac{1}{2} - \tfrac{1}{4}(x_i - x_{i-1})/((x_{i-1} - x_{i-2}) + (x_i - x_{i-1}))\}\phi_i \\ & + \{\tfrac{1}{2} + \tfrac{1}{4}(x_i - x_{i-1})/(x_{i-1} - x_{i-2})\}\phi_{i-1} \\ & + \{[(\tfrac{1}{2}(x_i - x_{i-1}) + \tfrac{1}{4}(x_i - x_{i-1})^2/(x_{i-1} - x_{i-2}))/ \\ & \quad ((x_{i-1} - x_{i-2}) + (x_i - x_{i-1}))] \\ & - \tfrac{1}{2}(x_i - x_{i-1})/(x_{i-1} - x_{i-2})\}\underset{\text{source}}{\phi_{i-2}};\end{aligned} \tag{6}$$

For $u < 0$:

$$\begin{aligned}\phi_e = {} & \{\tfrac{1}{2} - \tfrac{1}{4}(x_{i+1} - x_i)/((x_{i+2} - x_{i+1}) + (x_{i+1} - x_i))\}\phi_i \\ & + \{\tfrac{1}{2} + \tfrac{1}{4}(x_{i+1} - x_i)/(x_{i+2} - x_{i+1})\}\phi_{i+1} \\ & + \{[(\tfrac{1}{2}(x_{i+1} - x_i) + \tfrac{1}{4}(x_{i+1} - x_i)^2/(x_{i+2} - x_{i+1}))/ \\ & \quad ((x_{i+2} - x_{i+1}) + (x_{i+1} - x_i))] \\ & - \tfrac{1}{2}(x_{i+1} - x_i)/(x_{i+2} - x_{i+1})\}\underset{\text{source}}{\phi_{i+2}},\end{aligned} \tag{7}$$

$$\begin{aligned}\phi_w = {} & \{\tfrac{1}{2} + \tfrac{1}{4}(x_i - x_{i-1})/(x_{i+1} - x_i)\}\phi_i \\ & + \{[(\tfrac{1}{2}(x_i - x_{i-1}) + \tfrac{1}{4}(x_i - x_{i-1})^2/(x_{i+1} - x_i))/ \\ & \quad ((x_{i+1} - x_i) + (x_i - x_{i-1}))] \\ & - \tfrac{1}{2}(x_i - x_{i-1})/(x_{i+1} - x_i)\}\phi_{i+1} \\ & - \{\tfrac{1}{4}(x_i - x_{i-1})/((x_{i+1} - x_i) + (x_i - x_{i-1}))\}\phi_{i-1} + \underset{\text{source}}{\tfrac{1}{2}\phi_{i-1}}.\end{aligned} \tag{8}$$

Each of these expressions locally satisfies our general one-dimensional quadratic polynomial. The source terms in equations (5)–(8) are implemented like those in equations (1)–(4). REBUFFS allows for a uniform or non-uniform grid by computing control-volume dimensions from input grid point co-ordinates.

Several additional minor modifications to the original REBUFFS code of LeQuere *et al.*[7] have been made. These modifications include restructuring the code to a modular format, optimizing for operation on an IBM-3081 computer, and the ability to interface with graphic routines.

Problem definition and execution information

The three-dimensional cavity flow simulation presented below used a nonuniform grid of $32 \times 32 \times 45$ for the half-cavity. Simulating the half-cavity flow only is valid and cost-effective, because the experimental results show a symmetric flow about the centre plane of the lateral span.[15] The numerical boundary condition imposed at the centre plane is that of a no-flux surface.

The calculations were performed at the IBM Palo Alto Scientific Center (PASC) on an IBM-3081 running under the VM operating system. Approximately 8 megabytes of core were required for this simulation. The time step size for the transient solution ranged from 0·02 s for the initial start-up phase to a maximum of 10·0 s. The average number of iterations per 10·0 s time step was 150. The implementation of the non-uniform QUICK scheme increased execution times by only 39 per cent above that of the original HYBRID formulation.

A comparison of execution time with two other three-dimensional codes indicate that REBUFFS' required cpu time is competitive. REBUFFS required approximately 0·8 ms per iteration-cell. The TURBIT-3 code, an explicit finite difference code,[16] consumes approximately 0·3 ms per time step-cell when executing on an IBM-3033. The TEMPEST code,[17] also an explicit finite difference code based on TEACH-like principles, uses an estimated 0·5 ms per time step-cell on a CDC-7600. It is possible to convert these execution times to equivalent IBM-3081 cpu time.[18] This results in a TURBIT-3 estimate of about 0·3 ms per time step-cell and for TEMPEST about 1 ms per time step-cell. Naturally, these approximate cpu times are only general indicators of execution costs.

COMPARISON OF EXPERIMENT AND SIMULATION

The experimental results are for a *Re* of 3300 and reproduced from Reference 15. The computed results are at a time of 20 min and for a *Re* of 3200. The simulation *Re* of 3200 was chosen to match the experiment when laser-Doppler velocity measurements were obtained (to be discussed later). The difference in *Re* between the visualization experiment and the velocity measurement experiment is due to the fluid temperature on the day of the particular experiment, but is of no consequence in this comparison.

The computed fields are displayed in vector plots and particle track plots. The vector plots are normalized by the largest vector in the plane displayed. The particle tracks are generated from the 20 min instantaneous velocity fields which are assumed constant for the 5–8 s during which the particle tracks are computed. The depth-of-field for the particle track plots varies from 2 to 4 mm as it did in the experiment photographs.

Figures 4 and 5 display the general flow structure within the cavity. This pattern is generated by the motion of the belt which drags adjacent fluid. Eventually this dragged fluid collides with the downstream vertical wall and is deflected downward. A secondary eddy is formed in the apex of the vertical and bottom boundaries as a result of frictional losses and stagnation pressure.

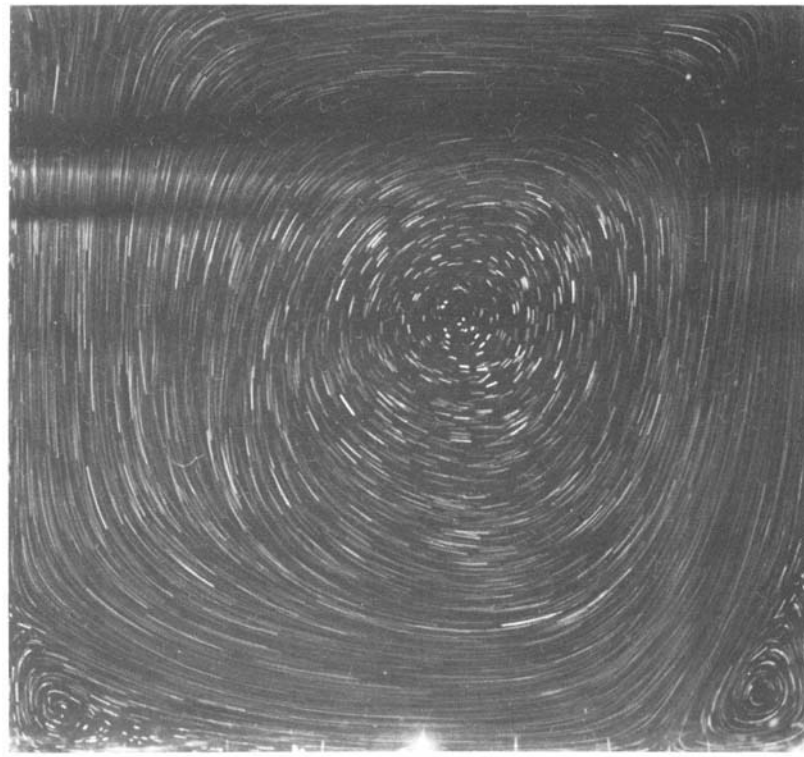

Figure 4. Flow in Plane 40 mm from end-wall

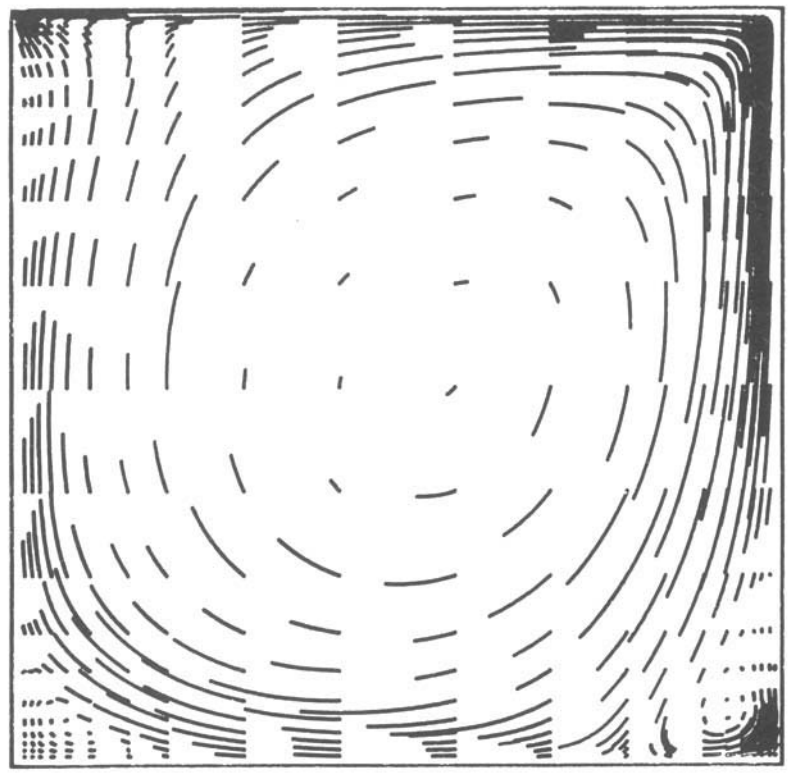

Figure 5. Particle tracks for flow in plane 40 mm from end-wall

The primary circulating fluid continues towards the upstream vertical wall, generating another secondary eddy in the upstream lower corner. The circulation loop is closed when the fluid is re-entrained by the lid. The experimentally observed spanwise variation in the flow field structures is reproduced by the simulated results. Corner eddy size is influenced by proximity to the end-wall and location of the TGL vortices. As one would expect the no-slip condition at the end-wall drains energy from the velocity field, modifying the location and size of eddy structures.

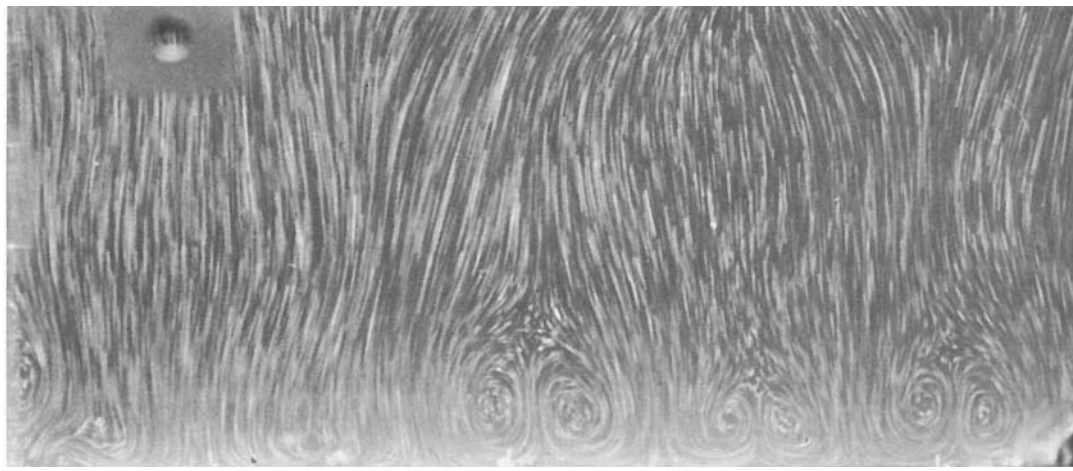

Figure 6. Flow in plane 35 mm upstream of downstream wall

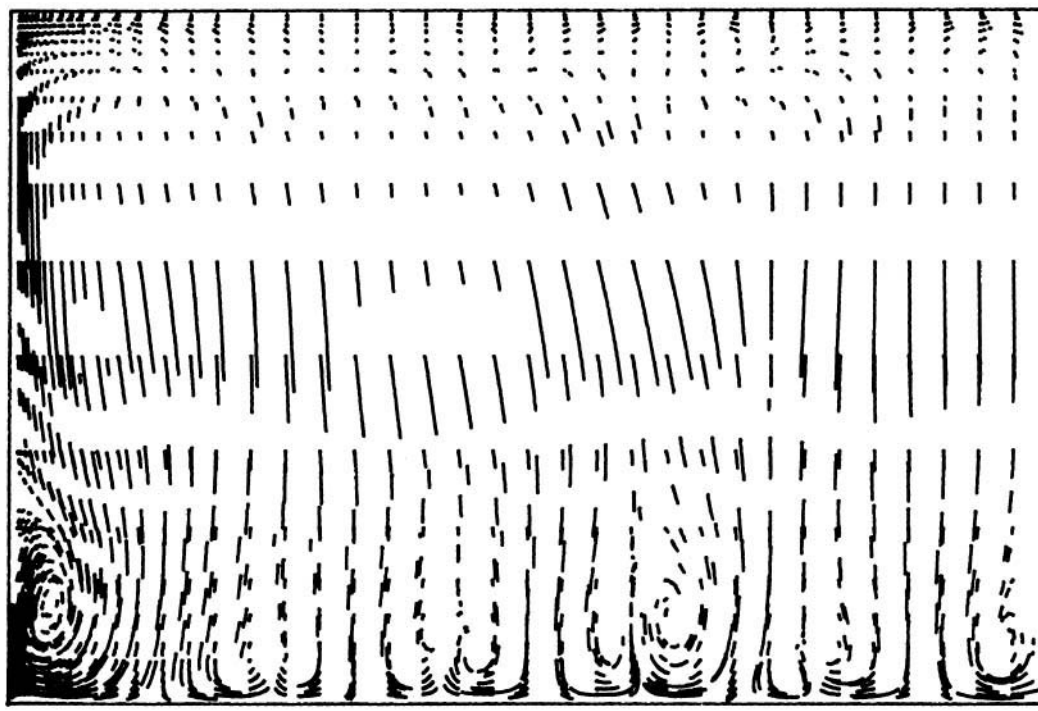

Figure 7. Particle tracks for flow in plane 35 mm upstream of downstream wall

Figure 6 gives experimental results at a plane 35 mm from the downstream wall, QTMS in Figure 2, which displays the presence of the corner vortex and four pairs of TGL vortices. The corresponding simulated plane is reproduced in Figures 7 and 8. The simulated field also possesses a corner vortex and four pairs of variable-sized TGL vortices. The numerical generation of the TGL vortices did not require a random perturbation of the velocity fields, but rather the presence of the end-wall is sufficient to instigate their development. The formation of the corner vortex induces a rotational effect which slowly propagates out from the end-wall. This effect in combination with the concave shape of the surface representing the interface between the primary circulation cell and downstream corner eddy (see Figure 2) generates the TGL vortices.

Figures 9 and 10 demonstrate the variation in corner vortex and TGL vortices strength and size due to spatial location. Figures 9 and 10 are at a plane 75 mm from the downstream wall. The corner vortex does not penetrate to the bottom of the cavity and quite noticeable secondary motions are present in the centre and at the top of the cavity. The motions at the top of the cavity could be the vestiges of the TGL vortices convected by the dominant primary circulation or the fluid response to the vortex in the upper left corner of the cavity. As one would suspect, the strength of the TGL vortices is dependent on their proximity to the downstream wall. In Figures 9 and 10, which are more isolated from the downstream wall than Figures 7 and 8, the TGL vortices appear to be slightly larger or more fully developed, but a more quantitative analysis is required to verify this.

The downstream corner eddy size, as shown in Figures 2, 4 and 5, appears to be correlated to whether the planes parallel to the symmetry plane fall between TGL vortices or intersect a TGL vortex pair. If the downstream eddy intersects a TGL vortex pair, this results in a weaker recirculation due to significant local spanwise motions generated by the TGL vortex pair. A less

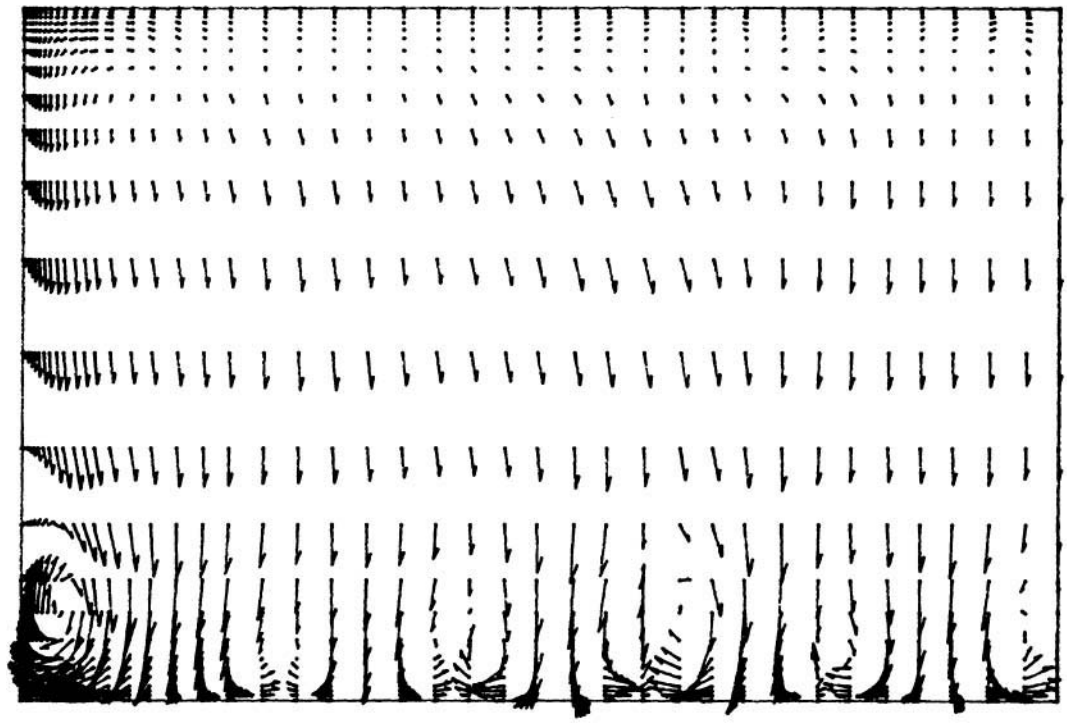

Figure 8. Vector field for flow in plane 35 mm upstream of downstream wall

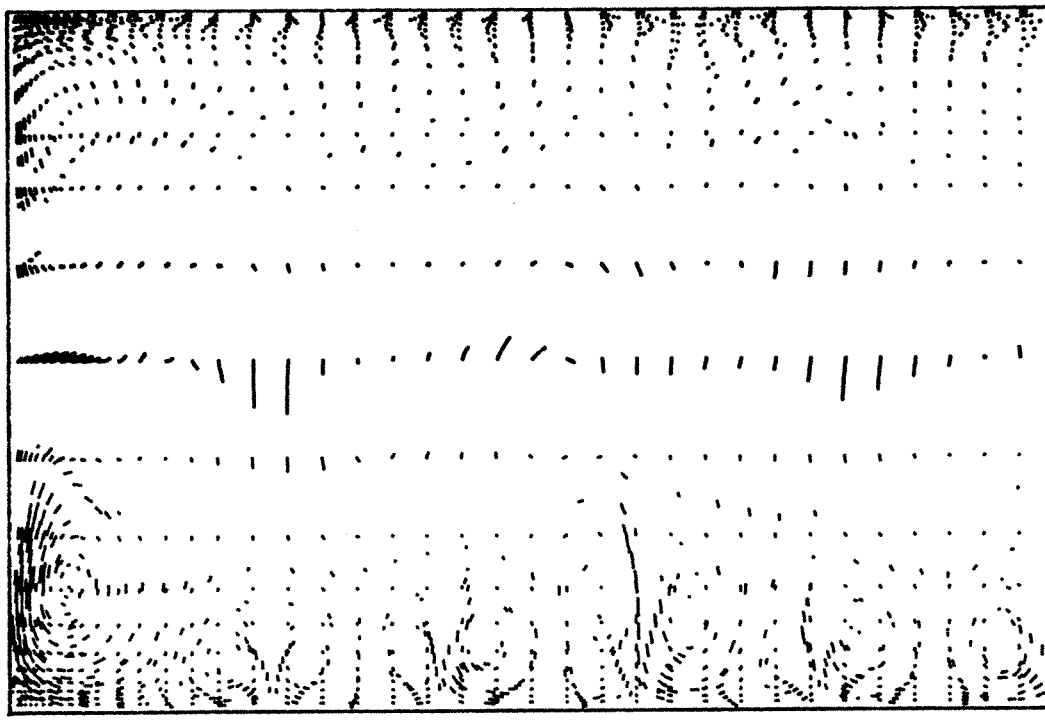

Figure 9. Particle tracks for flow in plane 75 mm upstream of downstream wall

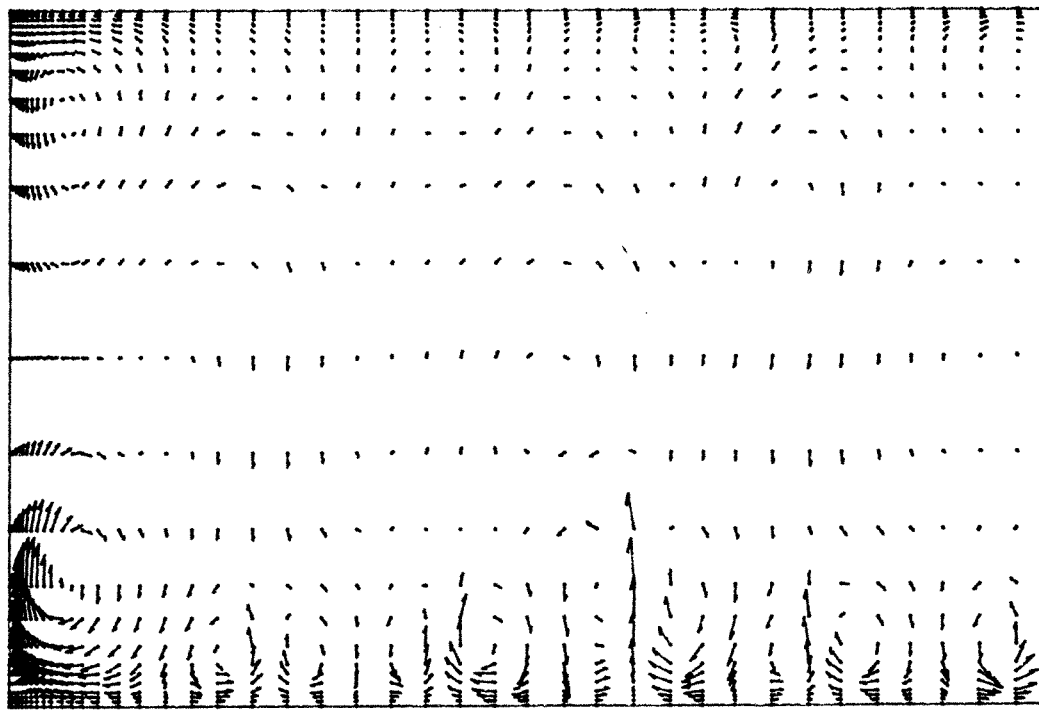

Figure 10. Vector field for flow in plane 75 mm upstream of downstream wall

well defined downstream secondary eddy results. A stronger downstream eddy exists when the plane containing the eddy falls between TGL vortices. Thus, local spanwise motions generated by TGL vortices do modify flow structure in planes perpendicular to these motions. Additionally, as was noted first in the experiment and then in the simulation, the location and size of TGL vortices is very dynamic and possibly periodic.[15] In order to determine this periodicity further analysis will be required.

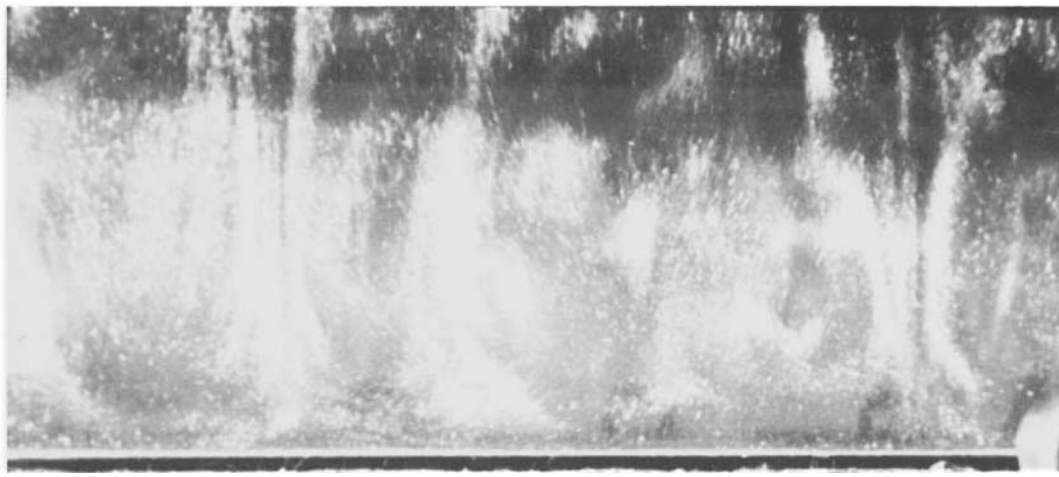

Figure 11. Flow in plane 5 mm from upstream wall

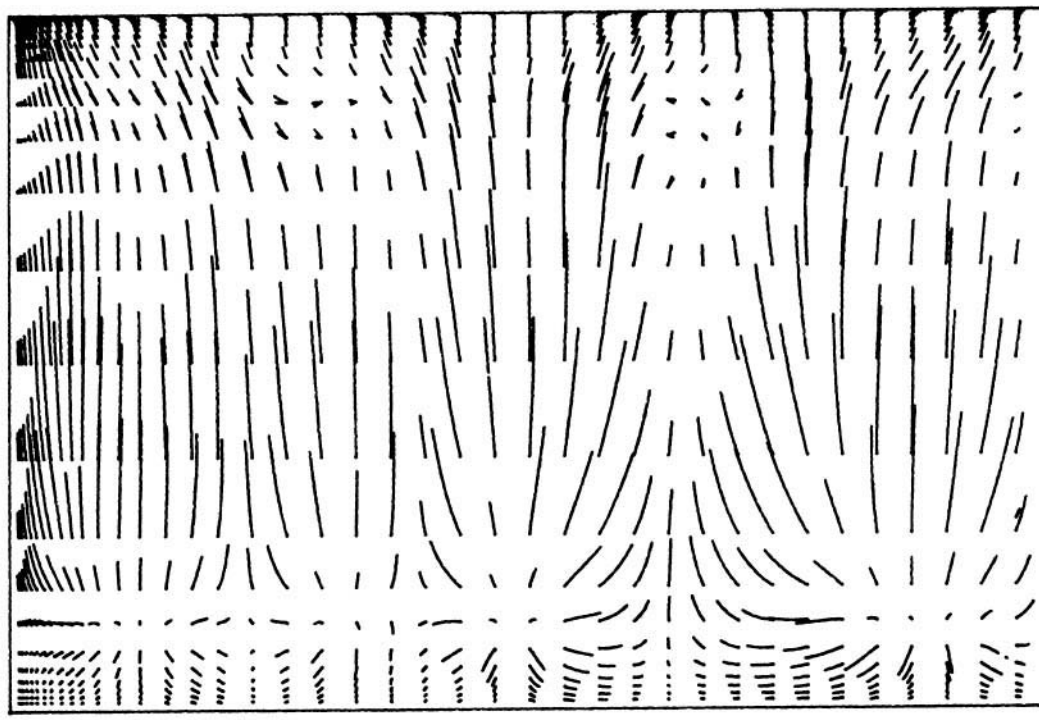

Figure 12. Particle tracks for flow in plane 5 mm from upstream wall

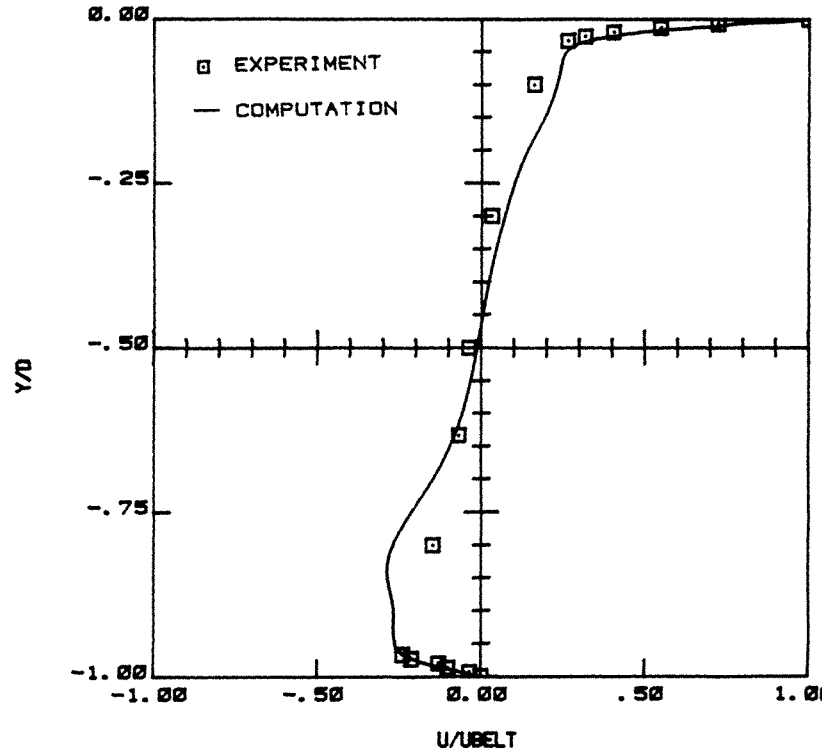

Figure 13a. Normalized mean U velocity profiles at symmetry plane for $Re = 3200$

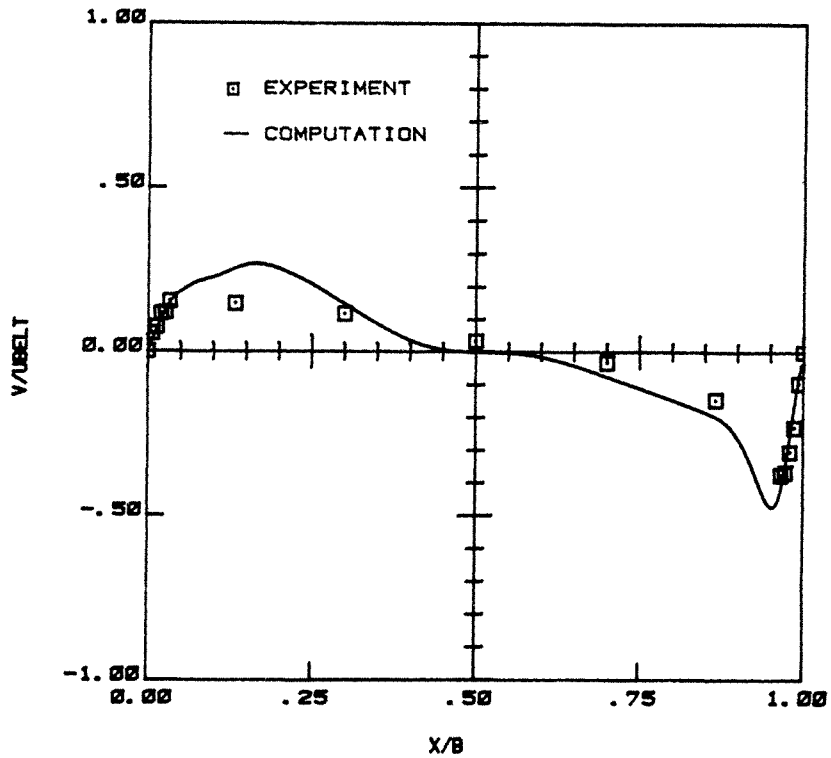

Figure 13b. Normalized mean V velocity profiles at symmetry plane for $Re = 3200$

Figure 11 displays the streakline pattern induced by the TGL vortices at a plane 5 mm from the upstream side-wall (plane PKNR in Figure 2). The similar effect for the computed fields is reproduced in the particle track plot of Figure 12. In Figure 11 the influence of the TGL vortices concentrates particles of the rheoscopic liquid (the light zones). The corresponding phenomenon occurs in Figure 12. Note that the line representing the interface between the primary circulation cell and the upstream secondary eddy is seen in Figure 12 near the bottom of the cavity.

The final comparison is of the traditional normalized (by the belt velocity) mean velocity profile plot at the symmetry plane on the appropriate centrelines (Figures 13(a), (b)). The experimental data points represent five-minute sample averages, whereas the computed profiles are three-minute sample averages begun at the 20 minute mark of the flow. Three-minute averages for the computed profiles were used because the running means were constant. As previously mentioned the influence of the TGL vortices modifies the flow structure in the symmetry plane in some periodic manner. In addition, the numerical no-flux boundary condition at the symmetry plane influences the computed velocity profiles in a manner absent in the experiment (the symmetric flow assumption requires further investigation). Therefore, we would not expect complete agreement of experiment and simulation. Yet, we do see the similar general shape of the profiles, both being drastically different to the profiles generated by two-dimensional simulations.[1,19]

CONCLUSIONS

The improvement of the global accuracy of REBUFFS by introducing a modified QUICK formulation coupled with an effective non-uniform grid has been sufficient to generate successful numerical results for the three-dimensional laminar lid-driven cavity flow. The experimentally observed TGL longitudinal vortices, as well as other general flow structures, have been simulated for the half-cavity. The total impact of the presence of the TGL vortices has not been assessed, but preliminary results indicate that they strongly modify the flow structure. Also, the size and location of the TGL vortices is time-dependent.

The assessment of the quasi-periodic structure of the three-dimensional cavity flow will be the focus of one aspect of our group's future work. Further numerical simulations of the three-dimensional cavity flow will include investigation of the impact of thermally unstable convection on the overall flow structure and studies of thermally influenced turbulent flow.

ACKNOWLEDGEMENTS

The authors wish to thank Professor J. A. C. Humphrey at the University of California, Berkeley for suppling the three-dimensional REBUFFS code. Computer support was supplied by the IBM Palo Alto Scientific Center (PASC) of the IBM Corp. through a Research Support Program agreement with RLS. Software support on the IBM-3081 was given by Dr. D. Shieh of IBM. This work was primarily performed in the Environmental Fluid Mechanics Laboratory at Stanford University. The research project is supported by the Hydraulics, Hydrology, and Water Resources Engineering Program, National Science Foundation through Grant No. CEE-7921324 and by the Division of Engineering, Mathematical and Geosciences, Office of Basic Energy Sciences, Department of Energy through contract No. DOE-DE-AT03-81-ER-10867.

REFERENCES

1. J. R. Koseff and R. L. Street, 'Visualization studies of a shear driven three-dimensional recirculating flow', *Three-Dimensional Turbulent Shear Driven Flows, ASME*, 1982, pp. 23–31.

2. H. S. Rhee, J. R. Koseff and R. L. Street, 'Flow visualization of a recirculating flow by rheoscopic liquid and liquid crystal techniques', *Experiments in Fluids*, **2**, 57–64 (1984).
3. J. R. Koseff, R. L. Street, P. M. Gresho, C. D. Upson, J. A. C. Humphrey and W.-M. To, 'A three-dimensional lid-driven cavity flow: experiment and simulation', *Proc. 3rd Int. Conf. Num. Meth. Lam. and Turb. Flow*, Seattle, August 1983.
4. B. P. Leonard, 'A stable and accurate convective modeling procedure based on quadratic upstream interpolation', *Computer Methods in Applied Mechanics and Engineering*, **19**, pp. 59–98, (1979).
5. B. P. Leonard, 'A stable, accurate, economical and comprehendible algorithm for the Navier–Stokes and scalar transport equations', *Numerical Methods in Laminar and Turbulent Flow, 2nd International Conference*, Venice, Italy, 13–16 July 1981, pp. 543–554.
6. K. B. Katsaros, W. T. Liu, J. A. Businger and J. E. Tillman, 'Heat transport and thermal structure in the interfacial boundary layer measured in an open tank of water in turbulent free convection', *J. Fluid Mech.*, **83**, (2), 311–335 (1977).
7. P. LeQuere, J. A. C. Humphrey and F. S. Sherman, 'Numerical calculation of thermally driven two-dimensional unsteady laminar flow in cavities of rectangular cross section', *Numerical Heat Transfer*, **4**, 249–283 (1981).
8. A. D. Gosman and W. M. Pun, 'Lecture notes for course entitled calculation of recirculating flows', *No. HT5/74/2*, Imperial College, London, 1974.
9. S. V. Patankar, and D. B. Spalding, 'A calculation procedure for heat, mass and momentum transfer in three-dimensional parabolic flows', *Int. J. Heat and Mass Transfer*, **15**, 1787–1806 (1972).
10. S. V. Patankar, *Numerical Heat Transfer and Fluid Flow*, McGraw-Hill, New York, 1980.
11. P. J. Roache, *Computational Fluid Dynamics*, Hermosa Publishers, 1982.
12. T. Han, J. A. C. Humphrey and B. E. Launder, 'A comparison of HYBRID and quadratic-upstream differencing in high Reynolds number elliptic flows', *Computer Methods in Applied Mechanics and Engineering*, **29**, 81–95 (1981).
13. A. Pollard and A. L. W. Siu, 'The calculation of some laminar flows using various discretisation schemes', *Computer Methods in Applied Mechanics and Engineering*, **35**, 293–313 (1982).
14. B. P. Leonard, Private communication, 19 July 1983.
15. J. R. Koseff, 'Momentum transfer in a complex recirculating flow', *Ph.D. Dissertation*, Department of Civil Engineering, Stanford University, California, 1983.
16. G. Grötzbach, 'Spatial resolution requirements for numerical simulation of internally heated fluid layers', *Numerical Methods in Laminar and Turbulent Flow, 2nd International Conference*, Venice, Italy, 13–16 July 1981.
17. D. S. Trent, L. L. Eyler and M. J. Budden, 'TEMPEST, A three-dimensional time-dependent computer program for hydrothermal analysis, volume I: numerical methods and input instructions', *Pacific Northwest Laboratory Report PNL-4348 Vol. I*, September 1983.
18. J. J. Dongarra, 'Performance of various computers using standard linear equations software in a Fortran environment', *ANL Technical Memo*, 24 October 1983.
19. U. Ghia, K. N. Ghia and C. T. Shin, 'Solution of incompressible Navier–Stokes equations by coupled strongly implicit multi-grid method', *Symposium on Multigrid Methods*, NASA-AMES Research Center, California, October 1981.